View metadata, citation and similar papers at core.ac.uk
brought to you by CORE
provided by University of Queensland eSpace

5th Australasian Congress on Applied Mechanics, ACAM 2007
10-12 December 2007, Brisbane, Australia

Metal-Polymer Functionally Graded Materials for Removing Guided Wave Reflections at Beam End Boundaries

C.K. Liew[1], M. Veidt[1], D.T. Chavara[2], A.J. Ruys[2], C. Young[2], M. McCreery[2]

[1]*Division of Mechanical Engineering, University of Queensland, Brisbane, QLD 4072, Australia*
[2]*School of Aerospace, Mechanical and Mechatronic Engineering J07, University of Sydney, Sydney, NSW 2006, Australia*

Abstract: This paper investigates the potential of a metal-polymer functionally graded material (FGM) to remove beam end boundary wave reflections that produce complicated interference patterns in the response signals used for guided wave damage identification methodologies. The metal-polymer FGM matches the material properties to a metal beam for total wave transmission on one side and is continuously graded to a viscoelastic polymer on the other side. An Aluminium-Polycarbonate (Al-PC) FGM was fabricated and characterised using microscopy, hardness testing and through-transmission ultrasonics to verify the continuous gradient. Measurements of guided waves on an aluminium beam attached to the FGM on one end show reduction in boundary wave reflections that varies with wave frequency. A damaged aluminium beam attached with the FGM produced promising improvements in a damage identification system.

Keywords: functionally graded material, guided wave ultrasonics, structural health monitoring, neural network, pattern recognition.

1 Introduction

Guided wave ultrasonics has attracted a lot of attention in recent years as a promising non-destructive evaluation technique due to its high sensitivity to discontinuities and its ability to propagate large distances with small amounts of energy, hence resulting in a cost-effective damage evaluation and structural health monitoring tool. However, signal processing of the transient wave response for accurate quantification of damages in structures remains a challenging procedure. One of the challenges is the superposition of scattered wave pulses from damages with reflections from structural boundaries which result in complex interference patterns.

Numerical methods to separate different travelling wave modes exist [1] but their applications are limited to waves not influenced by factors like noise and mode coupling that are usually present in practice. An alternative that is independent of these factors is to physically remove the boundary wave reflections from the structure. Attempts to attenuate wave reflections in steel plates and beams with a discretely graded impedance end interface has shown that the reflected wave energy can be damped by 60%-80% in plates and 60%-90% in beams [2]. These results motivate the investigation of functionally graded materials (FGMs) to further improve the removal of boundary wave reflections.

An FGM is a two-component composite whose composition varies from one component to the other in a continuous manner. Continuous bulk FGMs have been successfully fabricated at the Centre for Advanced Materials Technology at the University of Sydney using an Impeller Dry Blending (IDB) process [3,4]. The IDB process works by controlled blending the powder forms of the two material components and gradually depositing the continuously graded composition in a mold for densification. In a collaboration effort, the centre has produced Aluminium-Polycarbonate (Al-PC) FGMs [5]. The FGM matches the material properties of the metal beam for total wave transmission on one side and of a viscoelastic polymer for wave energy dissipation on the other side. Figure 1 shows a picture of the Al-PC FGM used in this project.

Figure 1. Picture of the Al-PC FGM where light areas are aluminium while dark areas are polycarbonate.

2 Characterising the Continuous Gradient

Prior to using the FGM into a guided wave application, its gradient was verified with three material characterisation methods, viz. optical microscopy, hardness testing and ultrasonic through-transmission testing. The test region for microscopy and hardness testing was the polished 50mm long flat surface of a 35mm diameter cylindrical FGM cut in half along its longitudinal axis. For ultrasonic through-transmission testing, the FGM was further cut and polished into a 12mm thick rectangular block.

2.1 Microscopy

A JVC TK-1280E colour video camera was integrated with a microscope [5] to capture photos in series longitudinally along the gradient of the FGM. 12x magnification was set on the microscope where each image captured covered an area of approximately 3mm x 2mm of the test region. A total of 16 images were captured, which spanned an area of approximately 48mm x 2mm along the gradient. These images were stored and examined using Leica QWin, an image processing and analysis tool for microscopy. The images were converted into greyscale to distinguish between light and dark areas, which composed of Aluminium (Al) and Polycarbonate (PC) regions respectively, Figure 2(a). The Leica QWin program was then used to detect the percentage of light areas over the total area of the image. Figure 2(b) shows the results for the 16 images plotted in sequence longitudinally along the FGM with a coefficient correlation of 0.988. The approximately linear trend in % Al clearly verifies the continuous change in composition along the gradient of the FGM.

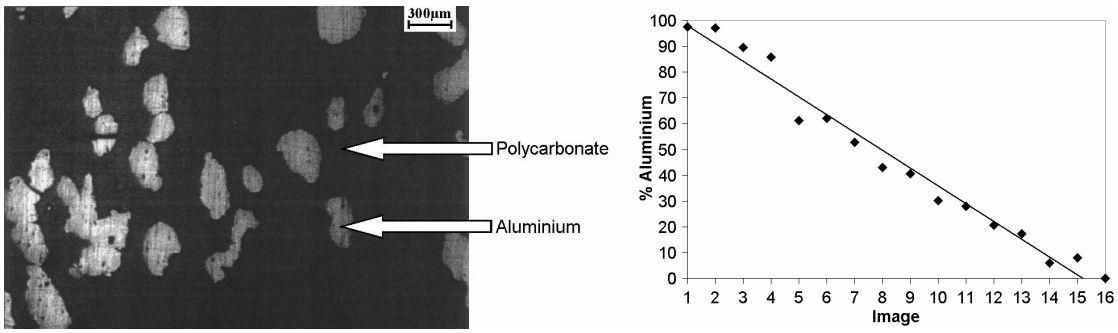

(a) (b)

Figure 2. (a) Sample greyscale photo showing light and dark areas, indicating aluminium and polycarbonate regions respectively. (b) Linear trend in % aluminium verifies the continuous change along the FGM gradient.

2.2 Hardness Testing

A PTC Type D Durometer with a 30° angle conical cone indenter was used for hardness testing [6]. The Durometer is a compact handheld instrument that is pressed onto the surface of the specimen in which displaces a needle on an analogue dial to show the Durometer Hardness Number. Durometers are commonly used to characterise rubbers and plastics but was used for testing the FGM since the material proved to be too soft even at the 100% Al region for Brinell, Rockwell and superficial Rockwell hardness testing methods [5]. This was an early indication of a different microstructure in the FGM due to incomplete densification, which will be discussed later in this paper. Despite substantial scatter, the Durometer results with a coefficient correlation of 0.918 in Figure 3 show that there is a gradual change from a softer to a harder material along the FGM gradient.

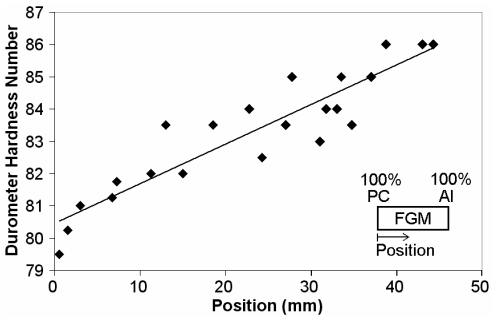

Figure 3. Durometer Hardness Number along the length of the FGM gradient.

2.3 Ultrasonic Through-Transmission Testing

The third test involved the use of a transducer and a Pinducer that were both connected to a Panametrics Model 5072 Pulser/Receiver. The transducer transmitted 5MHz longitudinal wave pulses through the 12mm thickness of the FGM specimen from one surface, which were received by the Pinducer on the opposite surface. Wave pulse signals detected by the Pinducer were displayed on an oscilloscope, which allowed the determination of the travelling time of the pulse through the FGM thickness. It was then possible to calculate the longitudinal bulk wave velocity, an acousto-ultrasonic material property with relevance to the FGM application for guided wave ultrasonics.

Figure 4 shows the average results from 10 measurements with standard deviation limits. The expected lower and upper bounds are calculated from rule of mixture estimations [7] using material properties listed in Table 1. The gradual change in density, stiffness and Poisson's ratio is illustrated by the increase in the wave velocity as a function of increased Al content. However, the results are below the expected linear change in composition with the exception of the measurement for 100% PC. The 5% lower than expected wave velocity at 100% Al is another indication of a mismatch between the Al side of the FGM and Al structures manufactured from conventional techniques like extrusion and casting. The influence of this mismatch on the transmission behaviour of guided waves is described later in this paper.

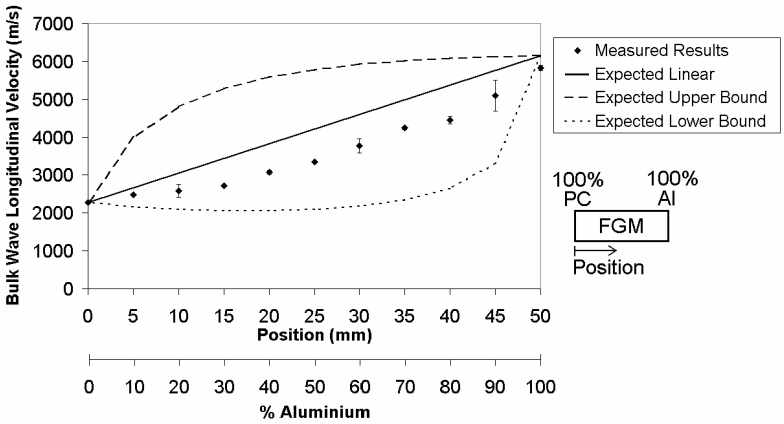

Figure 4. Average bulk wave velocities along the FGM gradient with the expected upper and lower bounds.

3 Application of the FGM in Guided Wave Ultrasonics

3.1 Experimental Setup

The FGM was machined into a 50mm x 12mm x 6mm rectangular block and its Al side was adhesively bonded to one end of a 2000mm x 12mm x 6mm Al beam. The PC side was bonded to a viscoelastic 100mm x 12mm x 6mm polyurethane (PU) block, Figure 5. The highly attenuative properties of PU would require a much shorter and practical length of PU compared to PC as the damping material. A piezoceramic transducer bonded to the far end of the Al beam was used to generate narrow band tone burst longitudinal wave pulses. A Polytec OFV 303/PFV 3001 laser vibrometer system was used to measure the transient wave response at the centre of the 6mm thickness surface of the beam.

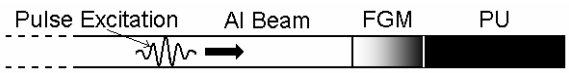

Figure 5. The Al-FGM-PU beam specimen for experiments.

Table 1 shows the mechanical properties of the individual materials in the Al-FGM-PU beam specimen. The wave velocity, c, was approximated by comparing the change in incident pulse arrival times measured at several locations along the length of each material. These velocities were lower than theoretical group velocities in rods due to the influence of complex dispersion in rectangular beams that cannot be quantified through an exact solution [8]. Nevertheless, these velocity approximations were adequate in developing accurate simulations for pattern recognition [9]. The acoustic impedance, Z, defined in (1), was used to determine the wave reflection and transmission coefficients at the interfaces, C_R and C_T respectively, according to (2) [10].

Table 1. Properties of materials in the Al-FGM-PU beam specimen.

Material	Density, ρ (kg/m^3)	Wave Velocity, c (m/s)	Impedance, Z (MRayls)
Aluminium (Al)	2700	4750	12.83
Polycarbonate (PC)	1200	2200	2.64
Polyurethane (PU)	1100	1900	2.09

$$Z = \rho\, c \tag{1}$$

$$C_R = \frac{Z_2 - Z_1}{Z_1 + Z_2}\ ,\ C_T = \frac{2Z_2}{Z_1 + Z_2} \tag{2}$$

3.2 Reflected Wave Energy in Undamaged Beam

The transient wave responses for a range of pulse centre frequencies were measured in the middle of the Al beam. From the wave velocity in Table 1, the arrival times of the incident and reflected pulses were known while the centre frequency determined the pulse length. Equal lengths of incident and reflected pulses were extracted from the signal based on the individual pulse arrival times and Fourier transformed into the frequency domain. The area under the magnitude of the Fourier transformed signal gave the energy of the respective wave pulses. The % reflected energy was obtained by comparing the wave energies of the reflected pulse to the incident pulse. Measurements and signal processing were repeated 10 times for each frequency. The average results with error limits are plotted in Figure 6(a). Measurements were made only within the working frequency range of the damage identification system described in the next section. The 'ideal' horizontal line shown in the figure was determined based on the polycarbonate-polyurethane reflection coefficient at the FGM-PU interface, assuming total wave transmission at the Al-FGM interface.

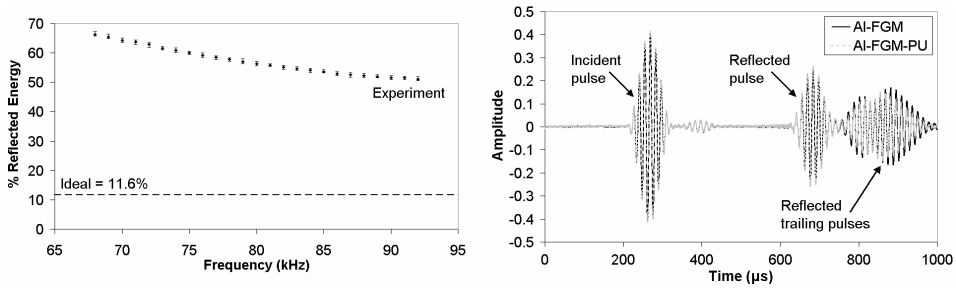

(a) (b)

Figure 6. (a) The % reflected wave energy from the Al-FGM-PU beam varies with frequency. (b) Comparison between Al-FGM and Al-FGM-PU measured transient wave signals at 70kHz.

Although the error limits show high consistency in the experimental results within each frequency, the reflected energy vary with frequency and are much larger than the predicted ideal calculation. The dependency of the reflected energy to frequency is attributed mainly to wave dispersion [8]. To investigate the discrepancy in magnitudes, the PU block was removed from the beam specimen and response signals were measured. Figure 6(b) shows a comparison between Al-FGM and Al-FGM-PU signals. It is found that the PU damping material has almost no influence on the reflected wave energy since it only results in a small reduction in the amplitude of the reflected trailing pulses. This suggests that only a small proportion of the wave pulse is transmitted into the PU block and the remaining larger proportion of the pulse is reflected back into the Al beam from the FGM.

The FGM was densified by cold pressing in a hydraulic press and heated to 180°C in an oven in cycles [5]. At this sintering temperature, only PC powder turned into a coherent mass while the Al particles were left cold welded and pressure bonded. Increasing the temperature further to sinter the Al powder was not possible, as this would have gone pass the melting point of PC. The partially sintered Al side of the FGM caused a mismatch in properties at the Al-FGM interface and thus, total wave transmission was not achieved. Guided wave energy that successfully transmitted through the interface then encountered the highly porous microstructure and uneven composition along lateral planes within the FGM, as shown in Figure 1, causing complex internal wave reflections, rotations and interferences. These effects combined with the mismatch at the Al-FGM interface result in a relatively large first reflected pulse and trailing pulses, as evident in Figure 6(b).

3.3 Application in a Damage Identification System

A damage identification system using neural network pattern recognition [9] was used to test the potential of the FGM in improving damage quantification accuracies. For damage identification, a full-width step damage of 40mm x 2mm was manufactured at the centre of the Al beam.

3.3.1 Experimental and Simulated Patterns

Laser vibrometer measurements were taken 10mm away from the transducer-Al interface for excitation centre frequencies 70kHz, 80kHz and 90kHz. Time signals that spanned from the onset of the incident pulse to the end of the reflected pulse from the Al-FGM interface were extracted for each frequency. The modulus of these signals were decomposed with the discrete wavelet transform in dyadic scales until the 5th level through a wavelet derived filter bank from the 8th order Daubechies wavelet [11]. These wavelet patterns were required to preserve signal features while reducing the number of sampling points for faster neural network computation.

Simulated wavelet patterns were used to train the neural network for identifying the experimental patterns. Patterns were generated for varying single damages on the beam identified by the damage location, depth and length. The simulation assumes the damage region as an inhomogeneity [12], which applies the reflection and transmission coefficients from (2) at the damage boundaries and the interfaces. Two sets of simulations were produced where the FGM was assumed to give either ideal total wave transmission or frequency dependent reflected wave proportion following Figure 6(a).

3.3.2 Neural Network

Pattern recognition was performed using a multi-layer perceptron feedforward backpropagation neural network. A parallel network system [13] was adopted with a total of three collaboratively linked neural networks, each network processing only patterns observed from one excitation centre frequency. Each network also utilised test pattern dependent techniques [9] for optimising the network weights and selecting accurate predictions. All the networks follow the same architecture consisting of a single hidden layer that was designed using a systematic approach [14]. The design of the network is summarised in Table 2. Neural network training was performed using MATLAB® with the terms used in Table 2 described accordingly in its neural network toolbox manual [15].

Table 2. Neural network design.

Inputs	Hidden Neurons	Outputs	Transfer Function	Backpropagation	Error	Validation	Validation Patterns	Training Patterns
28 (Wavelet Coefficients)	10	3 (Damage Parameters)	Hyperbolic Sigmoid	Resilient	Mean Square	Early Stopping	2423 (Simulated)	4845 (Simulated)

3.3.3 Results

Neural network test results are presented in Figure 7. Results without the FGM-PU segment attached to the Al beam are also shown for the comparison of damage identification performance.

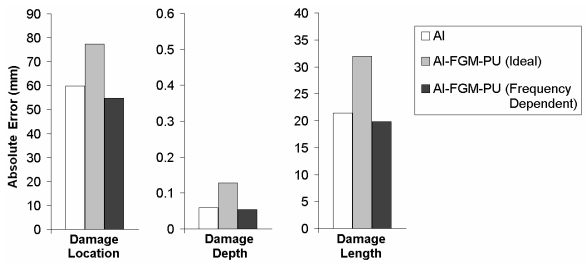

Figure 7. Pattern recognition damage identification performance for the three damage parameters.

For a 2m long 6mm thick beam, it is clear from the bar graphs in Figure 7 that the pattern recognition damage identification system provided accurate predictions with absolute errors below 78mm, 0.13mm and 32.0mm for damage location, depth and length respectively for all three beam specimen configurations considered. The results show that trained neural networks that treated the FGM as an ideal material with total transmission of the incoming wave at the Al-FGM interface are less sensitive to the experimental patterns. This is seen as increases in absolute errors of around 18mm, 0.07mm and 10.5mm for damage location, depth and length respectively, when compared to results for the Al

beam specimen alone. However, improvements in accuracies are achieved by considering frequency dependent wave transmission in the FGM according to the results in Figure 6(a) with reduction of absolute errors of around 5mm, 0.005mm and 1.5mm for damage location, depth and length respectively. The results show the potential of applying the FGM to remove the boundary wave reflections in metal beams for the damage identification system. More accurate predictions can be achieved if the densification problem in the FGM is addressed and the reflected wave energy from the metal-FGM interface is reduced.

7 Conclusions and Recommendation

Microscopy, hardness testing and ultrasonic through-transmission testing have proven that there is a gradient in the continuous bulk FGM but with indications of below expected material properties around the Al regions due to high porosity from incomplete densification. This becomes more evident in reflected wave energy studies where the actual reflected energy varies with frequency and is more than 40% larger than the calculated constant ideal result in the 70kHz-90kHz frequency range considered. Despite these issues, the potential of FGM in a damage identification system has still been observed, showing improved accuracy for damage location, depth and length. The densification problems in metal-polymer FGMs can be addressed by more elaborate sintering and pressing procedures or other more advanced techniques like hydrostatic shock forming [3]. There are also continuing work to improve the IDB process for fabricating high quality FGMs in the future like the recently proposed screeding procedure to ensure even distribution of powders in the lateral layers [4].

References

[1] M. Staudenmann, *Structural Waves in Nondestructive Testing*, Doctor of Technical Sciences Thesis, Institute of Mechanics, Swiss Federal Institute of Technology, 1995.

[2] C. Vemula and A.N. Norris, Attenuation of Waves in Plates and Bars using a Graded Impedance Interface at Edges, *Journal of Sound and Vibration*, Vol. 196(1), 1996, pp. 107-127.

[3] B. Sutton, *Ceramic-Metal Functionally Gradient Materials*, Bachelor of Mechanical Engineering Thesis, School of Aerospace, Mechanical and Mechatronic Engineering, University of Sydney, 2004.

[4] D.T. Chavara and A.J. Ruys, Development of the Impeller-Dry-Blending Process for the Fabrication of Metal-Ceramic Functionally Graded Materials, *Advanced Ceramic Coatings and Interfaces: A Collection of Papers from the 30th International Conference on Advanced Ceramics and Composites*, 2006, pp. 311-319.

[5] M. McCreery, *Functionally Graded Materials,* Bachelor of Mechanical Engineering Thesis, School of Aerospace, Mechanical and Mechatronic Engineering, University of Sydney, 2006.

[6] American Society for Testing and Materials, D 2240-04 Standard Test Method for Rubber Property – Durometer Hardness, *Annual Book of ASTM Standards*, Vol. 09.01, 2005, pp. 424-436.

[7] W.D. Callister Jr, *Materials Science and Engineering: An Introduction*, John Wiley & Sons Inc., 2000.

[8] M.A. Medick, On Dispersion of Longitudinal Waves in Rectangular Bars, *Journal of Applied Mechanics*, Vol. 34, 1967, pp. 714-717.

[9] C.K. Liew and M. Veidt, Test Pattern Dependent Neural Network Systems for Guided Waves Damage Identification in Beams, *Proceedings of the 8th WSEAS International Conference on Neural Networks*, 2007, pp. 67-75.

[10] A.R. Selfridge, Approximate Material Properties in Isotropic Materials, *IEEE Transactions on Sonics and Ultrasonics*, Vol. SU-32, No. 3, 1985, pp. 381-394.

[11] C.K. Liew and M. Veidt, Evaluation of Laminar Defects in Beams using Guided Waves and Pattern Recognition Techniques, *Proceedings of the 1st International Conference on Structural Condition Assessment, Monitoring and Improvement*, 2005, pp. 231-238.

[12] C.H. Wang and L.R.F. Rose, Wave Reflection and Transmission in Beams Containing Delamination and Inhomogeneity, *Journal of Sound and Vibration*, Vol. 264, 2003, pp. 851-872.

[13] C.K. Liew and M.Veidt, Data Fusion in Test Pattern Dependent Parallel Neural Network Systems for Guided Waves Damage Identification in Beams, *Pattern Recognition Letters* (pending for review).

[14] C.K. Liew and M. Veidt, Optimization of Neural Network Pattern Recognition Systems for Guided Waves Damage Identification in Beams, *Review of Progress in Quantitative Nondestructive Evaluation*, Vol. 26, 2007, pp. 627-634.

[15] H. Demuth and M. Beale, *Neural Network Toolbox User's Guide*, MathWorks Inc., 2004.